ION CHANNELS

Molecular basis for pore blockade of human Na^+ channel $Na_v1.2$ by the μ-conotoxin KIIIA

Xiaojing Pan[1,2,3]*, Zhangqiang Li[1,2,3]*, Xiaoshuang Huang[1,2,3]*, Gaoxingyu Huang[1,2,3]*, Shuai Gao[4]†, Huaizong Shen[1,2,3], Lei Liu[2,4], Jianlin Lei[5], Nieng Yan[1,2,3]†‡

The voltage-gated sodium channel $Na_v1.2$ is responsible for the initiation and propagation of action potentials in the central nervous system. We report the cryo–electron microscopy structure of human $Na_v1.2$ bound to a peptidic pore blocker, the μ-conotoxin KIIIA, in the presence of an auxiliary subunit, β2, to an overall resolution of 3.0 angstroms. The immunoglobulin domain of β2 interacts with the shoulder of the pore domain through a disulfide bond. The 16-residue KIIIA interacts with the extracellular segments in repeats I to III, placing Lys^7 at the entrance to the selectivity filter. Many interacting residues are specific to $Na_v1.2$, revealing a molecular basis for KIIIA specificity. The structure establishes a framework for the rational design of subtype-specific blockers for Na_v channels.

The voltage-gated sodium (Na_v) channels are responsible for the rapid rising phase of an action potential and thus play an essential role in membrane excitability and electrical signaling (*1*–*4*). The Na_v channel complex usually consists of a core α subunit, encoded by *SCNxA* (x = 1 to 5, corresponding to $Na_v1.1$ to $Na_v1.5$, and x = 8 to 11 for $Na_v1.6$ to $Na_v1.9$, respectively), and one or two auxiliary β subunits (*5*, *6*). Whereas the α subunit is sufficient for voltage sensing and selective ion conductance, β subunits regulate the membrane localization of α subunits, modulate peak values of Na^+ current, and modify the kinetics of voltage-dependent channel activation and inactivation. Among the four characterized β subunits, all of which consist of an amino (N)–terminal immunoglobulin (Ig) domain, a single transmembrane (TM) helix, and an intracellular domain, β1 and β3 associate with α through noncovalent interactions, whereas β2 and β4 each form a disulfide bond with α (*6*–*10*).

Structures of complexes of $Na_v1.4$ with β1 from electric eels and humans show that the interface is conserved between these two species (*11*, *12*). Insight into the recognition of other β subunits comes mainly from mutagenic analysis and structural information for individual β subunits (*10*, *13*–*16*).

In addition to β subunits, Na_v channels are modulated by a myriad of natural toxins that are found in the venoms of various animals (*17*, *18*). There are generally two classes of toxins, pore blockers and gating modifier toxins (GMTs). The former, exemplified by guanidinium neurotoxin tetrodotoxin (TTX) and saxitoxin (STX), directly block ion conductance (*19*, *20*). The latter, usually peptides with lengths ranging from several residues to dozens of residues, bind to the voltage-sensing domains (VSDs) and alter the voltage-dependent gating properties of the channel (*17*). Some peptidic toxins, exemplified by the μ-conotoxins identified from cone snails, also act as pore blockers (*21*–*23*). The peptidic blockers can exhibit more stringent Na_v subtype specificity than the small-molecule pore blockers, hence representing leads of pharmacological interest because of the pathophysiological importance of Na_v channels (*24*, *25*).

Structures of an insect Na_v channel, Na_vPaS, alone and in complex with TTX, STX, and a GMT, Dc1a, reveal the molecular basis for the recognition and mode of action of these representative toxins (*26*, *27*). In an accompanying paper, we present the structures of human $Na_v1.7$ in complex with both β1 and β2 subunits, with the GMTs protoxin-II (ProTx-II) and TTX (yielding $Na_v1.7$-PT), and with huwentoxin-IV (HWTX-IV) and STX (yielding $Na_v1.7$-HS) (*28*). Yet, there was no structural information on the molecular recognition between Na_v channels and peptidic pore blockers.

Here, we present the cryo–electron microscopy (cryo-EM) structure of human $Na_v1.2$ bound to the μ-conotoxin KIIIA in the presence of the auxiliary subunit β2 ($Na_v1.2$-β2-KIIIA). $Na_v1.2$ that was originally isolated from rat brain, also known as a brain type-II Na_v channel, functions primarily in the central nervous system (*29*, *30*). Mutations in $Na_v1.2$ are associated with seizures, infantile spasms, and autism spectrum disorder (table S1) (*31*–*36*). $Na_v1.2$ is subject to almost irreversibly potent inhibition by KIIIA. Our structure reveals the molecular basis for the specificity of KIIIA for $Na_v1.2$.

Results

Cryo-EM analysis of human $Na_v1.2$ in the presence of β2 and KIIIA

The complex between human $Na_v1.2$ and β2 was coexpressed by using BacMam virus–infected human embryonic kidney (HEK) 293F cells and purified by following our recently reported protocol as described in the materials and methods in the supplementary materials (*12*) (fig. S1). The carboxy terminus–amidated KIIIA was chemically synthesized and folded by following a published protocol (*37*). The freshly purified $Na_v1.2$-β2 complex was concentrated to ~1 mg/ml and incubated with synthesized KIIIA (0.05 mg/ml) for 30 min before cryo-sample preparation. By following a standard pipeline for cryo-grid preparation, image acquisition, and data processing, we obtained an EM map to an overall 3.0-Å resolution from 200,275 selected particles. The resolution for the core region, including the density for KIIIA, was further improved to 2.9 Å after the application of a central mask during postprocessing (Fig. 1 and figs. S1 and S2).

Only the Ig domain of β2 was discernible, with resolution dropping from ~3.5 Å to 6 to 8 Å from the contact point with $Na_v1.2$ to the peripheral region (Fig. 1, A and B). The TM and intracellular segments were completely missing from the three-dimensional (3D) EM reconstruction. Characterization by mass spectrometry did not identify any fragments from the TM, likely because of their hydrophobic nature; however, it did identify several sequences predicted to belong to the intracellular domain, confirming the presence of the TM and the intracellular segment of β2 in the complex (fig. S3).

Model building was facilitated by the reported cryo-EM structure of human $Na_v1.4$, the crystal structure of β2-Ig, and the nuclear magnetic resonance structure of KIIIA [Protein Data Bank (PDB) codes 6AGF, 5FEB, and 2LXG, respectively] (*12*, *16*, *37*). For the 2005 residue–containing $Na_v1.2$, the resolved regions cover residues 117 to 1786 except for the extracellular loop (residues 285 to 313), the intracellular I-II linker (residues 442 to 739), and the II-III linker (residues 988 to 1190). All 16 residues in KIIIA were clearly resolved with unambiguous side chain assignment (Fig. 1B). The resolution of the β2-Ig domain was not sufficient for de novo model building. We therefore docked the crystal structure into the density as a rigid body with minor adjustment to the regions that were better resolved in the EM map (Fig. 1C and table S2).

Limited contacts between β2-Ig and $Na_v1.2$

The conformation of $Na_v1.2$ is nearly identical to that of $Na_v1.4$, with a root mean square

[1]State Key Laboratory of Membrane Biology, School of Life Sciences and School of Medicine, Tsinghua University, Beijing 100084, China. [2]Beijing Advanced Innovation Center for Structural Biology, School of Life Sciences and School of Medicine, Tsinghua University, Beijing 100084, China. [3]Tsinghua-Peking Joint Center for Life Sciences, School of Life Sciences and School of Medicine, Tsinghua University, Beijing 100084, China. [4]Department of Chemistry, Tsinghua University, Beijing 100084, China. [5]Technology Center for Protein Sciences, Ministry of Education Key Laboratory of Protein Sciences, School of Life Sciences, Tsinghua University, Beijing 100084, China.
*These authors contributed equally to this work. †Present address: Department of Molecular Biology, Princeton University, Princeton, NJ 08544, USA.
‡Corresponding author. Email: nyan@princeton.edu

deviation (RMSD) of 0.696 Å over 981 Cα atoms when the two structures are superimposed. All the functional entities, including the VSDs, the glyco-diosgenin–penetrated intracellular gate, and the position of the fast inactivation motif Ile-Phe-Met (IFM) on the III-IV linker, remain nearly unchanged (fig. S4).

The RMSD for the $Na_v1.2$-β2 and $Na_v1.7$-HS complexes is 0.76 Å over 944 Cα atoms. The β2-Ig domain in the $Na_v1.2$ complex almost completely overlaps with that in $Na_v1.7$-HS (*28*) (Fig. 1D). In addition to the previously identified disulfide bond between β2-Cys^{55} and $Na_v1.2$-Cys^{910} (*16*), which is located at the end of the extended helix of the fifth transmembrane segment (S5) in the second repeat ($S5_{II}$), the interface consists of a limited number of polar interactions (Fig. 1E). The side group of Tyr^{56} forms a hydrogen bond (H-bond) with the carbonyl oxygen (C=O) of Glu^{909}. Arg^{135} at the loop that connects β10 and β11 strands in β2-Ig appears to interact with the C=O groups of Asp^{917} and Cys^{918}, as well as the side chain carboxylate of Asp^{917}. However, the density for Arg^{135} was relatively poor in the EM map, indicating potential flexibility and less stable interaction around this area (fig. S5A). Other than this, no additional interface was observed between β2 and $Na_v1.2$. The limited contact may explain the dissociation of the $Na_v1.2$-β2 complex upon disruption of the disulfide bond (*13*). The lack of stable interaction with $Na_v1.2$ in the TM region may account for the invisibility of β2-TM in the EM reconstruction, which is in contrast to the extensive interactions between the well-resolved β1 and Na_vs (*11*, *12*, *28*).

Recognition of KIIIA by $Na_v1.2$

KIIIA contains 16 amino acids, among which six Cys residues form three disulfide bonds. Distinct isomers with different intradisulfide bond formations have been found in the synthesized and oxidative folding products of KIIIA, among which the major peak component, with the disulfide connectivity C1-C15, C2-C9, and C4-C16, represented the most potent blocker for $Na_v1.2$, with a dissociation constant K_d of ~5 nM (*37*). We faithfully reproduced the reported results for KIIIA synthesis and folding and added the major peak component to the purified $Na_v1.2$-β2 complex for cryo-sample preparation. The EM map unambiguously confirmed the three expected disulfide bonds in KIIIA (Fig. 2, A and B, and fig. S5B).

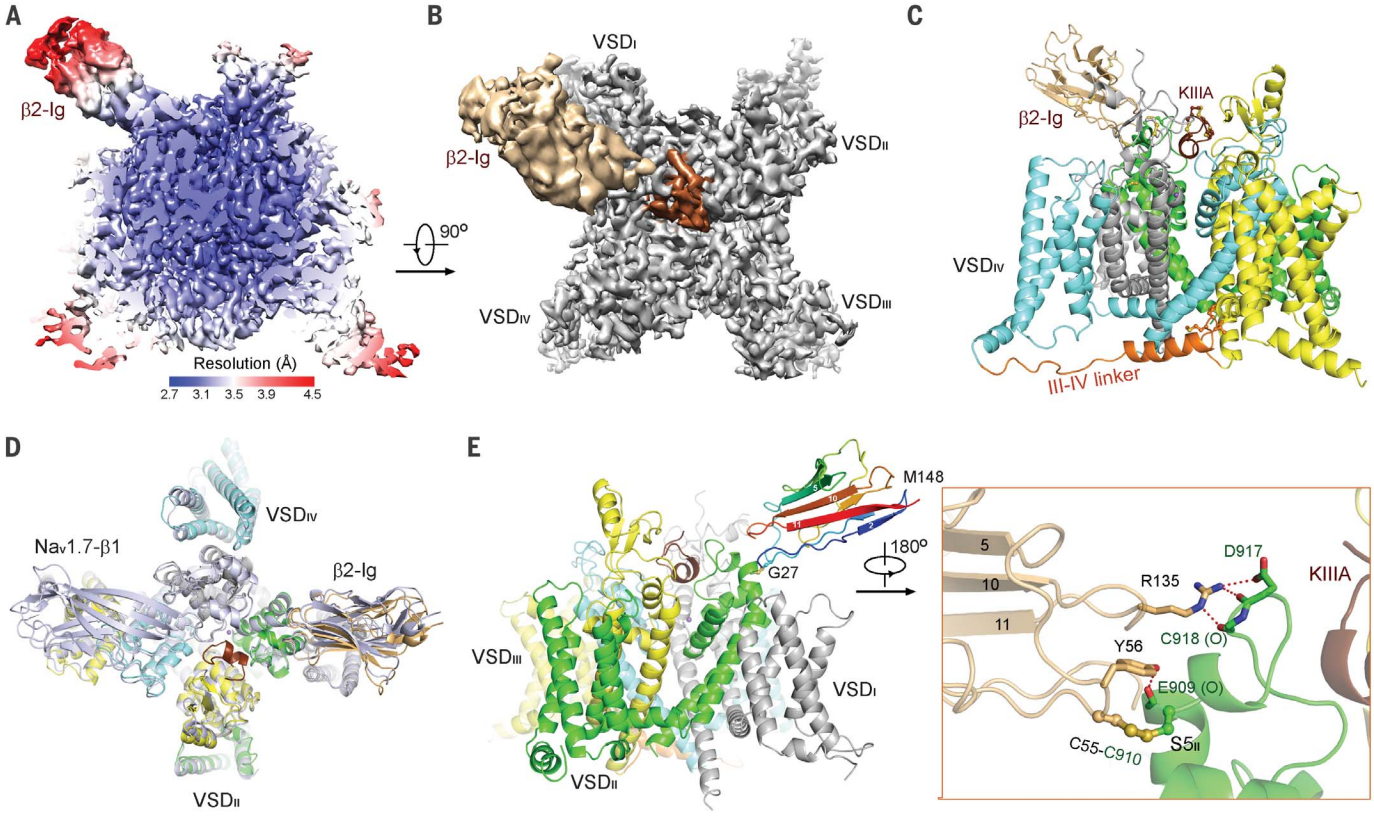

Fig. 1. Cryo-EM analysis of the human $Na_v1.2$-β2 complex bound to the μ-conotoxin KIIIA. (**A**) The 3D EM reconstruction of the complex at 3.0 Å resolution. Shown here is a cut-open view of the local resolution map calculated with RELION 2.1. Only the Ig domain of β2 was resolved to moderate resolutions. The intracellular segment, whose presence in the complex was confirmed by mass spectrometric analysis, and the TM helix were completely invisible. (**B**) KIIIA was unambiguously resolved in the complex. Shown here is an extracellular view of the EM map. The densities corresponding to KIIIA and β2 are colored brown and beige, respectively. The maps were generated in Chimera. (**C**) Overall structure of the human $Na_v1.2$-β2 complex bound to KIIIA. $Na_v1.2$ is domain colored. Disulfide bonds and the IFM fast inactivation motif are shown as balls and sticks. The Na^+ ion in the SF is shown as a purple sphere. Sugar moieties are not shown. All structure figures were prepared in PyMol (*40*). (**D**) Identical binding sites for β2-Ig on $Na_v1.2$ and $Na_v1.7$. The two β2-Ig domains are well overlaid in the superimposed structures of $Na_v1.7$-β1-β2 (light purple) in the presence of HWTX-IV and $Na_v1.2$-β2. (**E**) Limited contact between β2-Ig and the extracellular segments of $Na_v1.2$. (Left) β2-Ig is rainbow colored. The numbering of the β strands conforms to that of the crystal structure of β2-Ig (*16*), which was docked into the EM map as a rigid body. (Right) Interface between β2-Ig and $Na_v1.2$. The disulfide bond is shown as balls and sticks, and the putative polar interactions are represented by dashed lines. Single-letter abbreviations for the amino acid residues are as follows: A, Ala; C, Cys; D, Asp; E, Glu; F, Phe; G, Gly; H, His; I, Ile; K, Lys; L, Leu; M, Met; N, Asn; P, Pro; Q, Gln; R, Arg; S, Ser; T, Thr; V, Val; W, Trp; and Y, Tyr.

Despite the small surface area, the 16–amino acid (aa) toxin forms extensive polar interactions with the extracellular segments in repeats I, II, and III of $Na_v1.2$ (Fig. 2C and fig. S5C). On the top of the toxin in a side view, Asn^3 is H-bonded to Glu^{330} in repeat I (Fig. 2C, right). On one side of the toxin, the side chains of Lys^7, His^{12}, and Trp^8 are respectively coordinated by the side groups of Glu^{945} and Asp^{949} on pore helix 2 (P2) in repeat II ($P2_{II}$) and Tyr^{362} on the extracellular loop of repeat I (Fig. 2C, left, and fig. S5C). On the other side, the guanidinium group of Arg^{14} engages in a H-bond with the main chain C=O of Leu^{920}, as well as cation-π interaction with Tyr^{1443} on the extracellular loop of repeat II. Tyr^{1443} and Tyr^{1429} on $P2_{II}$ also sandwich Arg^{922} on repeat III for canonical cation-π interactions. Therefore, these loop regions are highly stabilized, with excellent density resolution (Fig. 2C, middle, and fig. S5C). Arg^{10} exhibits two conformers in the map (fig. S5D). In either conformation, the guanidinium group is coordinated by Asp^{1426} on $P2_{II}$ (Fig. 2C, left). In addition to the coordination with side chains, the backbone polar groups also contribute to the binding. The C=O groups of Asp^{11}, His^{12}, and Cys^{15} are H-bonded to the amide groups of Arg^{922}, Asn^{916}, and Met^{1374}, respectively (Fig. 2C, middle).

The structure provides the molecular details to account for the distinct inhibitory potencies of KIIIA on different Na_v isoforms. For instance, Zhang *et al.* showed that $Na_v1.2$ from rats is almost irreversibly blocked by KIIIA, whereas the median inhibitory concentration for the cardiac subtype $Na_v1.5$ from rats was estimated to be 284 μM (*21*). Among the seven residues whose side chains participate in KIIIA binding, three, which remain conserved in the respective human and rat homologs, vary between $Na_v1.2$ and $Na_v1.5$ (Fig. 2B). The sequence variations between $Na_v1.8$ and $Na_v1.2$ are even more marked (Fig. 2B). Consistently, $Na_v1.8$ was insensitive to KIIIA at up to 5 μM (*21*).

The replacement of Trp^8 with Ala markedly reduced the inhibitory potency of KIIIA for $Na_v1.2$ and $Na_v1.4$ (*21*). Trp^8 is H-bonded to Tyr^{362} in $Na_v1.2$. Whereas the corresponding locus is occupied by Tyr in seven human Na_v channels, it changes to His and Phe in $Na_v1.5$ and $Na_v1.8$, respectively. The reciprocal effects of these mutations on the inhibitory potency of KIIIA support the importance of the structurally revealed interaction between Trp^8 of KIIIA and Tyr^{362} of $Na_v1.2$ (Fig. 2C).

Molecular mechanism of pore blockade by KIIIA

The structure of $Na_v1.2$ bound to KIIIA elucidates the molecular basis for pore blockade. Our previous structural and molecular dynamics (MD) simulation analyses unveiled a Na^+ binding site constituted by the Asp and Glu residues from the Asp-Glu-Lys-Ala signature motif and an invariant Glu residue on the first helical turn of $P2_{II}$ (Asp^{384}-Glu^{942}-Glu^{945} in $Na_v1.2$, designated the DEE site) (*27*, *38*). A spherical density that is contiguous with the side group of Asp^{384} was resolved in the EM map (fig. S5E). This density feature is identical to that observed in the 2.6-Å-resolution map of Na_vPaS-Dc1a bound to TTX. A Na^+ ion was assigned into the DEE-surrounded density.

The overall surface contour of KIIIA is highly complementary to the funnel-shaped cavity enclosed by the extracellular segments in repeats I to III. Upon $Na_v1.2$ binding to KIIIA, a narrow gap can still lead to the entrance to the selectivity filter (SF) on the side of repeat IV (Fig. 3A). However, the bottleneck is blocked by the bottom tip of KIIIA, which plugs the cavity above the DEE site (Fig. 3B). Structural comparison with the Na^+ permeation path calculated from our previous MD simulation of Na_vPaS suggests that the bottom tip of KIIIA occupies the outer mouth to the SF (Fig. 3C).

The bottom tip of KIIIA is constituted by only one residue, Lys^7, whose side chain displays a fully extended conformation, with the amine group directly interacting with the Na^+-coordinating residue Glu^{945} (Fig. 3D). The linear Lys functions like a cork in the bottleneck, with the positively charged amine group effectively preventing the penetration of cations. The binding and action mechanism of KIIIA is reminiscent of the "lock and key" blockade of the $K_v1.2$-2.1 paddle chimera by charybdotoxin, wherein Lys^{27} of the toxin protrudes into the SF vestibule and blocks cation entrance (*39*) (fig. S6).

Structural superimposition with STX- or TTX-bound $Na_v1.7$ reveals that the amine group of Lys^7 in KIIIA coincides with 2-NH_2 of the 1,2.3-guanidinium of STX and C6-OH of TTX

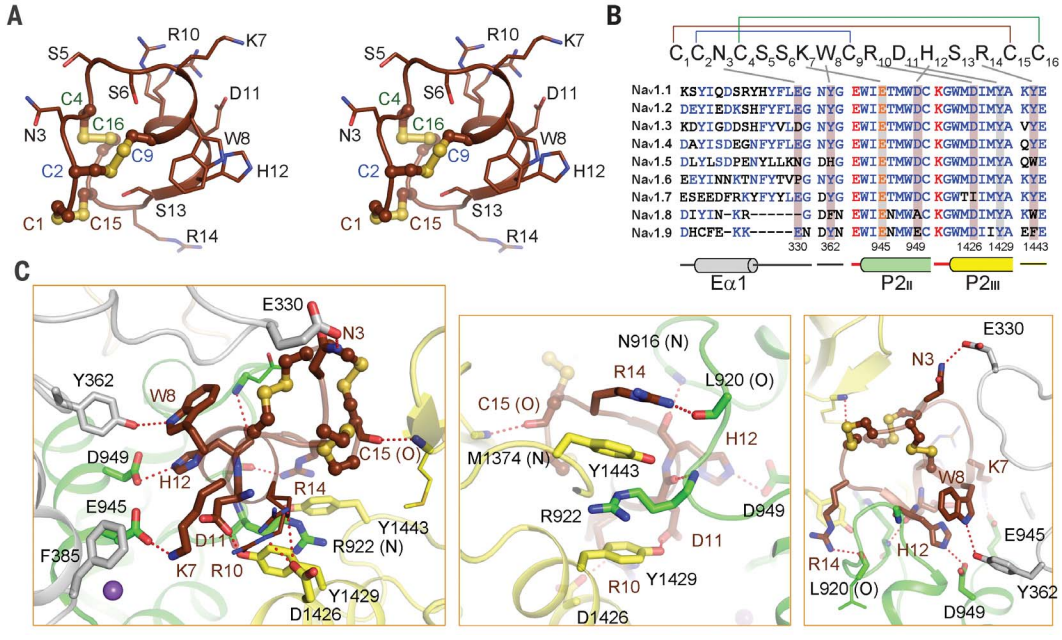

Fig. 2. Specific interaction between KIIIA and the extracellular segments of $Na_v1.2$. (**A**) Structure of KIIIA in the complex. The 16-aa toxin, shown in stereoview, is stabilized by three disulfide bonds. (**B**) The extracellular loops are less conserved among the nine human Na_v subtypes. (Top) The primary sequence of KIIIA. The intradisulfide bonds are indicated by colored lines on top of the sequence. (Bottom) Sequence alignment of the KIIIA-interacting residues in human Na_v channels. The sequence alignment was adapted from our recent publication (*12*). The residues whose side chains are involved in KIIIA coordination are shaded, and the interacting pairs between KIIIA and $Na_v1.2$ are indicated by gray lines between the sequences. Eα1, extracellular α helix 1. (**C**) Extensive polar interactions between KIIIA and the extracellular segments of $Na_v1.2$. (Left) Both side chains and backbone groups of KIIIA are coordinated by residues from repeats I to III of $Na_v1.2$. (Middle) π-cation interactions reinforce the binding between KIIIA and the extracellular loops in repeats II and III. (Right) Extracellular loops in repeat I contribute two H-bonds for KIIIA coordination. Repeat IV, which has no contact with KIIIA, is omitted in all panels for visual clarity.

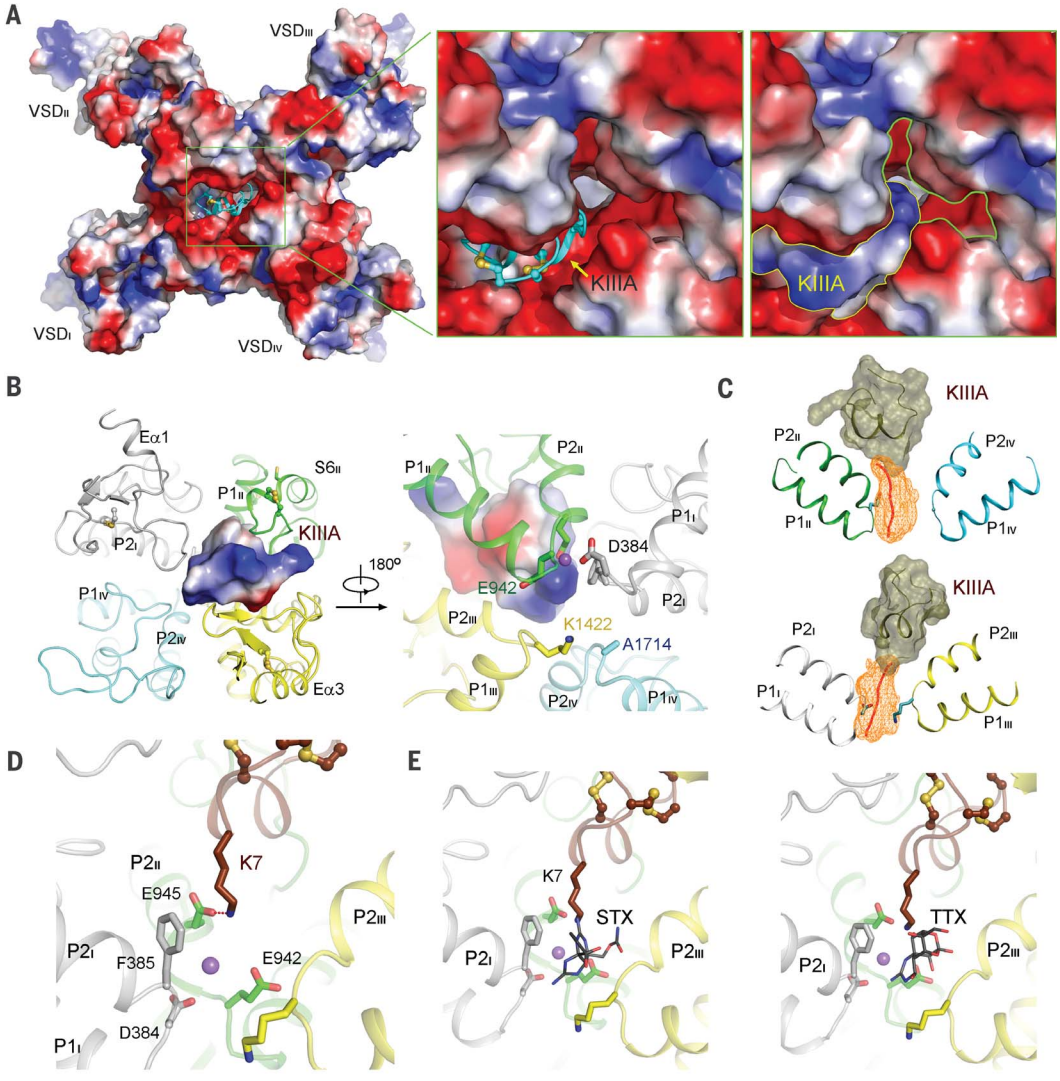

Fig. 3. Molecular basis for pore blockade by KIIIA. (**A**) The surface properties of KIIIA are highly complementary to the cavity enclosed by the extracellular segments in repeats I to III of $Na_v1.2$. Shown here is an extracellular view of the electrostatic surface potential of $Na_v1.2$ calculated in PyMol. KIIIA is shown as a cyan cartoon with the disulfide bonds shown as balls and sticks. The two insets, which are shown in identical views, illustrate the complementary contours and surface potentials of KIIIA and the extracellular cavity of $Na_v1.2$. The contours of KIIIA and the remaining gap in $Na_v1.2$ are indicated by yellow and green lines, respectively, in the right panel. (**B**) Asymmetric binding of KIIIA above the entrance to the SF. The extracellular and intracellular views of the SF and supporting P1 and P2 helices are shown. KIIIA is positioned above the DEE Na^+ binding site (purple sphere). (**C**) The bottom tip of KIIIA blocks the entrance to the SF. The structures of KIIIA-bound $Na_v1.2$ and Na_vPaS are superimposed. The contour envelope of the probability density map covering 80% of density points in the MD simulation of Na_vPaS is represented by orange wireframes (*38*). Shown here are the side views of the P1-SF-P2 segments from the indicated diagonal protomers. (**D**) Lys^7 of KIIIA blocks Na^+ entry to the Na^+ binding site within the SF vestibule. The DEE Na^+ binding site and Lys^7 are shown as sticks. (**E**) Comparison of pore blockade by KIIIA, STX, and TTX. Structures of STX- and TTX-bound $Na_v1.7$ are respectively superimposed with KIIIA-bound $Na_v1.2$. As the backbone and the side chains constituting the SF are completely identical between the two channels, only those in $Na_v1.2$ are shown. STX and TTX are shown as black thin sticks. Repeat IV is omitted in (D) and (E) for visual clarity.

despite the different binding sites for the peptidic blocker and the small-molecule blockers (Fig. 3E). Other than this overlapping, the overall structure of KIIIA is above STX and TTX (*27*, *28*).

Discussion

Aberrant function of $Na_v1.2$, one of the main Na_v subtypes in the brain, is associated with neurological and psychiatric disorders. Nearly 100 missense mutations in $Na_v1.2$ have been identified in patients with seizures, infantile spasm encephalitis, schizophrenia, and autism spectrum disorder (table S1). Structural determination of human $Na_v1.2$ allows mapping of these mutations, thereby providing a framework for functional and mechanistic investigations (fig. S7).

The structure of the human $Na_v1.2$-β2 complex bound to the peptidic pore-blocking μ-conotoxin KIIIA further expands the gallery of structures of Na_v channels associated with peptidic toxins (Fig. 4), including the insect Na_vPaS in complex with Dc1a (*27*); the human $Na_v1.7$ with two well-characterized tarantula toxins, HWTX-IV and ProTx-II (*28*); and now the human $Na_v1.2$ with KIIIA. In total, three different binding modes have been observed. Dc1a, HWTX-IV, and ProTx-II are all GMTs. Dc1a projects into the cavity enclosed by all four segments in VSD_{II} and the extracellular loop and $S5_{III}$ of the pore domain (Fig. 4, top right). Essentially, the pore domain provides the scaffold to anchor Dc1a, which then traps VSD_{II} in a particular conformational state. HWTX-IV and ProTx-II both bind to the peripheral region that links S3 and S4 in VSD_{II} (known as site 4 for toxins). ProTx-II also sits on top of the S3-S4 linker in VSD_{IV} (site 3). The relatively poor resolution of these toxins is likely due to the disruption of the lipid bilayer. The membrane, reminiscent of the pore domain for Dc1a, may provide anchorage to stabilize these peripheral GMTs, which then lock the functional states of the corresponding VSDs to modulate activation or inactivation of the channel.

KIIIA is a subtype-specific pore blocker with the most potent inhibitory effect on

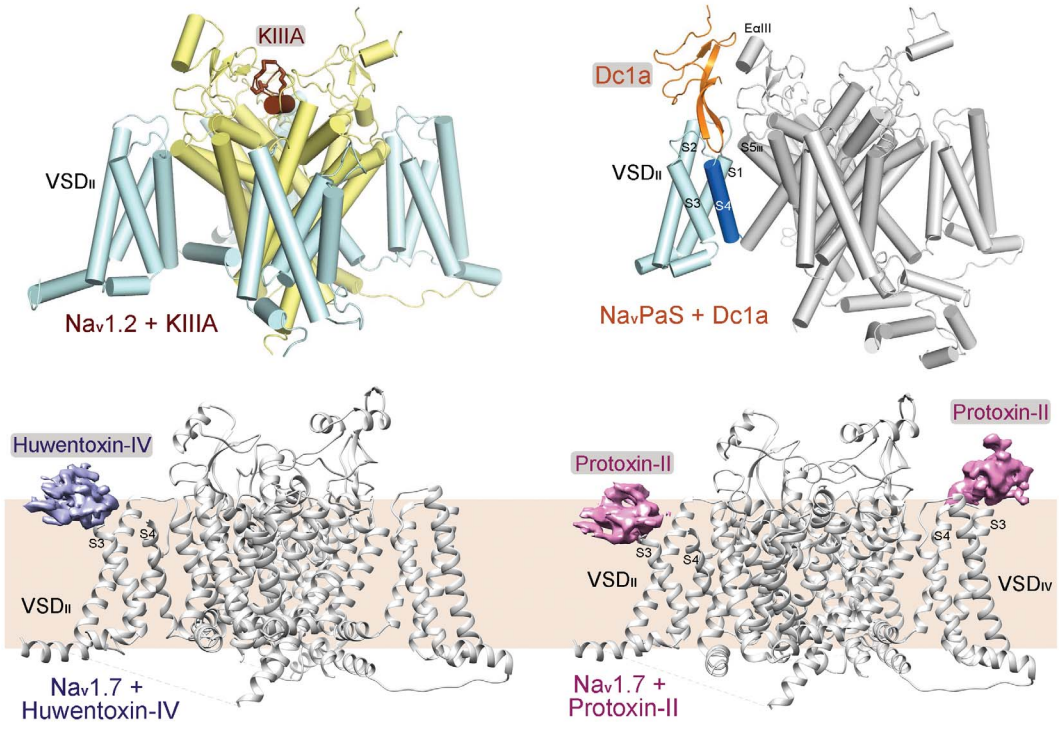

Fig. 4. Different modes of binding between peptidic toxins and Na_v channels. Shown here is a summary of available structures between Na_v channels and peptidic toxins. The PDB codes for the structures of Na_vPaS-Dc1a, $Na_v1.7$-HS, and $Na_v1.7$-PT are 6A90, 6J8G, and 6J8I, respectively. The densities for the GMTs HWTX-IV and ProTx-II and the structures of $Na_v1.7$ (*28*) were generated in Chimera. For visual clarity, the N-terminal domain of Na_vPaS is omitted and β subunits are not shown for $Na_v1.2$ and $Na_v1.7$.

$Na_v1.2$. Structural analysis shows that this is because many interacting residues are specific to $Na_v1.2$ (Fig. 2B). The extracellular sequences, which are much less conserved than the TM region of Na_v channels, may represent important sites for the development of subtype-specific drugs. Structural determination of human $Na_v1.2$, $Na_v1.4$, and $Na_v1.7$ and elucidation of the detailed interactions between KIIIA and $Na_v1.2$ will be valuable in the development of more specifically targeted therapeutics.

REFERENCES AND NOTES

1. A. L. Hodgkin, A. F. Huxley, *J. Physiol.* **104**, 176–195 (1945).
2. A. L. Hodgkin, A. F. Huxley, *J. Physiol.* **117**, 500–544 (1952).
3. B. Hille, *Ion Channels of Excitable Membranes* (Sinauer Associates, ed. 3, 2001), p. 814.
4. C. A. Ahern, J. Payandeh, F. Bosmans, B. Chanda, *J. Gen. Physiol.* **147**, 1–24 (2016).
5. A. L. Goldin *et al.*, *Neuron* **28**, 365–368 (2000).
6. H. A. O'Malley, L. L. Isom, *Annu. Rev. Physiol.* **77**, 481–504 (2015).
7. L. L. Isom *et al.*, *Science* **256**, 839–842 (1992).
8. L. L. Isom *et al.*, *Cell* **83**, 433–442 (1995).
9. K. Morgan *et al.*, *Proc. Natl. Acad. Sci. U.S.A.* **97**, 2308–2313 (2000).
10. F. H. Yu *et al.*, *J. Neurosci.* **23**, 7577–7585 (2003).
11. Z. Yan *et al.*, *Cell* **170**, 470–482.e11 (2017).
12. X. Pan *et al.*, *Science* **362**, eaau2486 (2018).
13. C. Chen *et al.*, *J. Biol. Chem.* **287**, 39061–39069 (2012).
14. J. Gilchrist, S. Das, F. Van Petegem, F. Bosmans, *Proc. Natl. Acad. Sci. U.S.A.* **110**, E5016–E5024 (2013).
15. S. Namadurai *et al.*, *J. Biol. Chem.* **289**, 10797–10811 (2014).
16. S. Das, J. Gilchrist, F. Bosmans, F. Van Petegem, *eLife* **5**, e10960 (2016).
17. W. A. Catterall *et al.*, *Toxicon* **49**, 124–141 (2007).
18. J. K. Klint *et al.*, *Toxicon* **60**, 478–491 (2012).
19. H. S. Mosher, F. A. Fuhrman, H. D. Buchwald, H. G. Fischer, *Science* **144**, 1100–1110 (1964).
20. C. Y. Kao, *Pharmacol. Rev.* **18**, 997–1049 (1966).
21. M. M. Zhang *et al.*, *J. Biol. Chem.* **282**, 30699–30706 (2007).
22. J. R. McArthur *et al.*, *Mol. Pharmacol.* **80**, 573–584 (2011).
23. E. Tosti, R. Boni, A. Gallo, *Mar. Drugs* **15**, 295 (2017).
24. B. R. Green, G. Bulaj, R. S. Norton, *Future Med. Chem.* **6**, 1677–1698 (2014).
25. W. Huang, M. Liu, S. F. Yan, N. Yan, *Protein Cell* **8**, 401–438 (2017).
26. H. Shen *et al.*, *Science* **355**, eaal4326 (2017).
27. H. Shen *et al.*, *Science* **362**, eaau2596 (2018).
28. H. Shen, D. Liu, K. Wu, J. Lei, N. Yan, *Science* **363**, 1303–1308 (2019).
29. R. P. Hartshorne, W. A. Catterall, *Proc. Natl. Acad. Sci. U.S.A.* **78**, 4620–4624 (1981).
30. R. P. Hartshorne, D. J. Messner, J. C. Coppersmith, W. A. Catterall, *J. Biol. Chem.* **257**, 13888–13891 (1982).
31. T. Sugawara *et al.*, *Proc. Natl. Acad. Sci. U.S.A.* **98**, 6384–6389 (2001).
32. H. Kodera *et al.*, *Epilepsia* **54**, 1262–1269 (2013).
33. K. Nakamura *et al.*, *Neurology* **81**, 992–998 (2013).
34. M. Saitoh *et al.*, *Epilepsy Res.* **117**, 1–6 (2015).
35. S. K. Sundaram, H. T. Chugani, V. N. Tiwari, A. H. M. M. Huq, *Pediatr. Neurol.* **49**, 46–49 (2013).
36. R. Ben-Shalom *et al.*, *Biol. Psychiatry* **82**, 224–232 (2017).
37. K. K. Khoo *et al.*, *Biochemistry* **51**, 9826–9835 (2012).
38. J. Zhang *et al.*, *Protein Cell* **9**, 580–585 (2018).
39. A. Banerjee, A. Lee, E. Campbell, R. Mackinnon, *eLife* **2**, e00594 (2013).
40. W. L. DeLano, The PyMOL Molecular Graphics System (2002); www.pymol.org.

ACKNOWLEDGMENTS

We thank X. Li (Tsinghua University) for technical support during EM image acquisition and C. Zhao and H. Deng at the Protein Chemistry Facility at the Center for Biomedical Analysis of Tsinghua University for mass spectrometric analysis of the protein sample. **Funding:** This work was funded by the National Key Basic Research (973) Program (2015CB910101) and the National Key R&D Program (2016YFA0500402 and 2017YFA0505200) from the Ministry of Science and Technology of China and by the National Natural Science Foundation of China (projects 31800628, 31621092, 31630017, 81861138009, and 91753205). We thank the Tsinghua University Branch of the China National Center for Protein Sciences (Beijing) for providing the cryo-EM facility support. We are grateful for the computational facility support on the cluster of Bio-Computing Platform (Tsinghua University Branch of the China National Center for Protein Sciences, Beijing) and the "Explorer 100" cluster system of Tsinghua National Laboratory for Information Science and Technology. N.Y. is supported by the Shirley M. Tilghman endowed professorship from Princeton University. **Author contributions:** N.Y. and X.P. conceived the project. X.P., Z.L., X.H., G.H., H.S., and J.L. performed the experiments. L.L. supervised the synthesis and oxidative folding of KIIIA. All authors contributed to data analysis. N.Y. wrote the manuscript. **Competing interests:** The authors declare no competing interests. **Data and materials availability:** The atomic coordinates and EM map have been deposited in the PDB and EMDB with the codes 6J8E and EMD-9780, respectively.

SUPPLEMENTARY MATERIALS

www.sciencemag.org/content/363/6433/1309/suppl/DC1
Materials and Methods
Figs. S1 to S7
Tables S1 and S2
References (*41–52*)

6 December 2018; accepted 29 January 2019
Published online 14 February 2019
10.1126/science.aaw2999